

# 10.1

## Synthetic Aperture Radar Algorithms

Ron Goodman and  
Walter Carrara  
*General Dynamics  
Advanced  
Information Systems*

1	Synthetic Aperture Radar Overview.....	1131
1.1	Image Resolution • 1.2 Synthetic Aperture Radar Imaging Modes •	
1.3	Examples of Synthetic Aperture Radar Imagery • 1.4 Characteristics of Synthetic Aperture Radar Signal Data • 1.5 Characteristics of Synthetic Aperture Radar Image Data	
2	Image Formation Algorithms .....	1139
2.1	History of Image Formation Algorithms • 2.2 Major Challenges in Synthetic Aperture Radar Image Formation • 2.3 Image Formation in the Stripmap Mode • 2.4 Image Formation in the Spotlight Mode	
3	Image Enhancement.....	1144
3.1	Autofocus Algorithms • 3.2 Impulse Response Shaping • 3.3 Other Image Enhancement Functions	
4	Image Exploitation.....	1148
4.1	Moving Target Detection • 4.2 Synthetic Aperture Radar Interferometry	
5	Chapter Summary.....	1152
	Acknowledgment .....	1152
	References.....	1152

This chapter presents a sampling of key algorithms related to the generation and exploitation of fine-resolution synthetic aperture radar (SAR) imagery. It emphasizes practical algorithms in common use by the SAR community. Based on function, these algorithms involve *image formation*, *image enhancement*, and *image exploitation*. Image formation transforms collected SAR data into a focused image. Image enhancement operates on the formed image to improve image quality and utility. Image exploitation refers to the extraction and use of information about the imaged scene.

Section 1 introduces the fundamental concepts that enable fine-resolution SAR imaging and reviews the characteristics of collected radar signal data and processed SAR imagery. These attributes determine the need for specific processing functions and the ability of a particular algorithm to perform such functions. Section 2 surveys leading SAR image formation algorithms and discusses the issues associated with their use. Section 3 introduces several enhancement algorithms for improving SAR image quality and utility. Section 4 samples image exploitation topics of current interest in the SAR community.

### 1 Synthetic Aperture Radar Overview

Radar is an acronym for *radio detection and ranging*. In its simple form, radar *detects* the presence of a target by sensing energy that the target reflects back to the radar antenna. It *ranges* the target by measuring the time interval between transmitting a signal (for instance, in the form of a short pulse) and receiving a return (the backscattered signal) from the target. Radar is an active sensor that provides its own source of illumination. Radar operates at night without impact and through clouds or rain with only limited attenuation.

A radar image is a two-dimensional (2D) map of the spatial variations in the radar backscatter coefficient (a measure of the strength of the signal returned to the radar sensor) of an illuminated scene. A scene includes targets, terrain, and other background. The image provides information regarding the position and strength of scatterers throughout the scene. While a common optical image preserves only amplitude, a radar image naturally contains phase and amplitude information. An optical sensor differentiates signals based on angle (in two dimensions) and makes no distinction based on

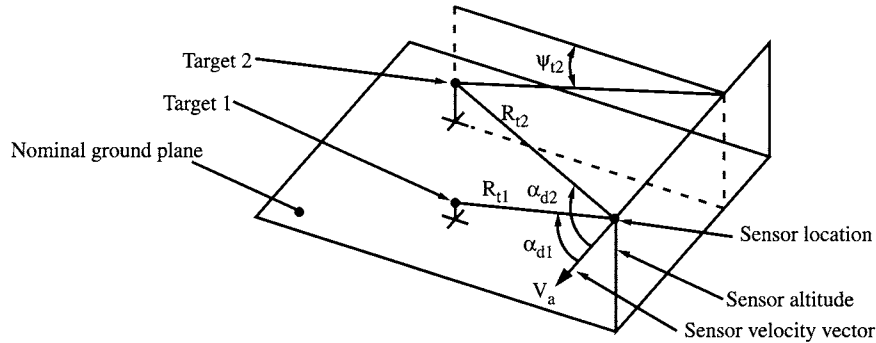
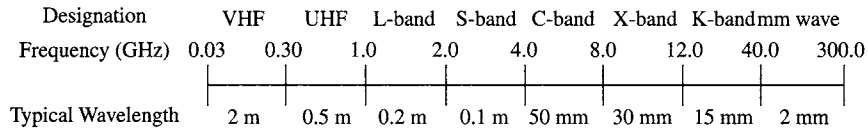
FIGURE 1 Resolution in range  $R_t$  and (Doppler) cone angle  $\alpha_d$ .

FIGURE 2 Frequency bands of synthetic aperture radar operation.

range to various scene elements. Imaging radar naturally separates returns in range and cone angle and does not differentiate signals based on depression (or elevation) angle. The (Doppler) cone angle  $\alpha_d$  is the angle between the radar velocity vector  $V_a$  (indicating the direction of antenna motion) and the line-of-sight vector from the antenna to a particular scatterer. The depression angle  $\psi_t$  is the angle between the horizontal plane and the projection of the line-of-sight vector onto a plane perpendicular to  $V_a$ . Figure 1 illustrates this range and angle differentiation by a SAR imaging system.

The ability to distinguish, or resolve, closely spaced features in the scene is an important measure of performance in an imaging system. In SAR imaging, it is common to define *resolution* as the  $-3\text{dB}$  width of the system impulse response function with separate measures in each dimension of the image. The  $-3\text{dB}$  width is the distance between two points, one on each side of the mainlobe peak, that are nearest to and one half the intensity of the peak.

The complex (phase and amplitude) nature of SAR imagery increases the ability of enhancement algorithms to improve the quality and interpretability of an image. It also increases the opportunity for image exploitation algorithms to derive additional information about an imaged scene. Traditional SAR provides 2D scatterer location and resolution between scatterers in range and azimuth (or cross-range). New applications extract three-dimensional (3D) information about the scene using interferometric techniques applied to multiple images of a scene collected from similar viewing geometries.

SAR imaging involves the electromagnetic spectrum in the frequency bands encompassing VHF through K-band. Figure 2 relates these frequency bands to radio frequency and

wavelength intervals. Various organizations throughout the world have successfully demonstrated and deployed SAR systems operating in most of these bands.

## 1.1 Image Resolution

Radar estimates the distance to a scatterer by measuring the time interval between transmitting a signal and receiving a return from the scatterer. Total time delay determines the distance to a scatterer; differential time delay separates scattering objects located at different distances from the radar sensor. The bandwidth  $B$  of the transmitted pulse limits time resolution to  $1/B$  and corresponding range resolution  $\rho_r$  to

$$\rho_r \approx \frac{c}{2B} \quad (1)$$

where  $c$  is the speed of light. To maintain high average power at the large bandwidths required for fine resolution, it is common to transmit a longer pulse with linear frequency modulation (FM) rather than a shorter pulse at constant frequency. Pulse compression following reception of the linear FM pulses achieves range resolution consistent with the transmitted bandwidth.

To generate a 2D image, the radar must separate returns arriving from the same distance based on differences in the angle of arrival. A real beam radar achieves this angular resolution by scanning a narrow illuminating beam across the scene to provide azimuth samples *sequentially*. Angular resolution is comparable to the angular extent of the physical beam. Synthetic aperture radar generates angular resolution much finer than its physical beamwidth. It transmits pulses

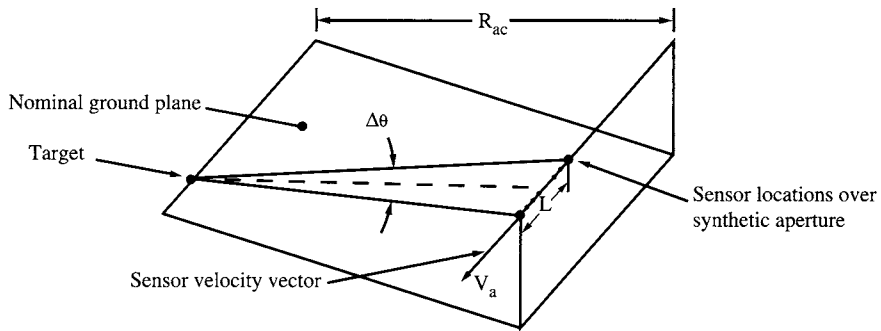


FIGURE 3 Synthetic aperture geometry.

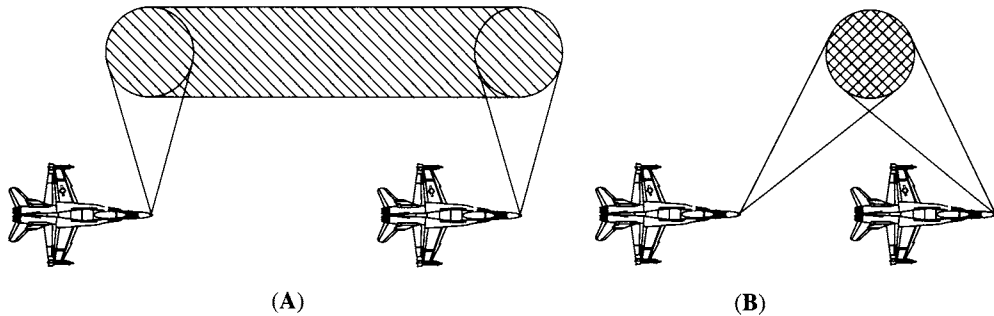


FIGURE 4 Basic synthetic aperture radar imaging modes: (A) Stripmap mode for area search and mapping; (B) spotlight mode for fine resolution.

from a series of locations along its trajectory (the synthetic aperture) and processes the collection of returns to synthesize a much narrower beam. The image formation processor (IFP) adjusts the relative phase among the returns from successive pulses to remove the phase effects of the nominally quadratic range variation to scatterers within the scene. It coherently sums the returns (generally via a Fourier transform) to form the synthetic beam and generate azimuth resolution cells. Signal processing provides azimuth samples *simultaneously* within a physical beamwidth.

The synthetic aperture concept is essential for achieving fine azimuth resolution when it is not practical to generate a sufficiently narrow real beam. The synthetic aperture provides an azimuth resolution capability  $\rho_a$  of

$$\rho_a \approx \frac{\lambda_c}{2\Delta\theta} \quad (2)$$

Here,  $\lambda_c$  is the center wavelength of the transmitted signal and  $\Delta\theta$  is the angular interval over which the processed data are collected. In SAR, unlike in real beam imaging, azimuth resolution is independent of the distance to scatterers in the scene.

Figure 3 illustrates this synthetic aperture geometry. As an example, consider a SAR system that collects signals over a synthetic aperture distance  $L$  of 1 km with an antenna moving at an along-track velocity  $V_a$  of 100 m/sec during a synthetic

aperture time interval  $T_a$  of 10 seconds. At a minimum range  $R_{ac}$  of 20 km, the synthetic aperture angular interval  $\Delta\theta$  is approximately 0.05 rad. With a transmitted bandwidth  $B$  of 500 MHz at a center wavelength of 0.03 m (X-band), these parameters offer azimuth resolution of 0.3 m and range resolution of 0.3 m.

## 1.2 Synthetic Aperture Radar Imaging Modes

Figure 4 illustrates two basic SAR data collection modes. In stripmap mode, the antenna footprint sweeps along a strip of terrain parallel to the sensor trajectory. Antenna pointing is fixed perpendicular to the flight line in a *broadside* collection, or pointed either ahead or behind the normal to the flight line in a *squinted* collection. The azimuth beamwidth of the antenna dictates the finest-achievable azimuth resolution by limiting the synthetic aperture, while the transmitted band width, sets range resolution by limiting the synthetic aperture. The antenna elevation beamwidth determines the range extent (or *swath width*) of the imagery while the length of the flight line controls the azimuth extent.

Stripmap mode naturally supports the coarser resolution, wide area coverage requirements of many natural resource and commercial remote sensing applications. Most airborne SAR systems include a stripmap mode. Remote sensing from orbit generally involves a wide area coverage requirement that necessitates the stripmap mode.

In spotlight mode, the antenna footprint continuously illuminates one area of terrain to collect data over a wide angular interval to improve azimuth resolution beyond that supported by the azimuth beamwidth of the antenna. Spotlight mode achieves this fine azimuth resolution at the cost of reduced image area. The angular interval over which the radar observes the scene determines azimuth resolution. Antenna beamwidths in range and azimuth determine scene extent.

Spotlight mode naturally supports target detection and classification applications that emphasize fine resolution over a relatively small scene. While a fine-resolution capability is useful largely in military and intelligence missions, it also has value in various scientific and commercial applications.

### **1.3 Examples of Synthetic Aperture Radar Imagery**

The following examples indicate the diversity of imagery and applications available from SAR systems. They include stripmap and spotlight mode images in a variety of frequency bands.

Figure 5 is a coarse resolution SAR image of Ft. Irwin, California, collected by the Canadian RADARSAT-1 satellite [1]. The RADARSAT-1 SAR operates at C-band (5.3 GHz) in the stripmap mode with a variety of swath width and

resolution options. The sensor collected this particular image at a resolution of 15.7 m in range and 8.9 m in azimuth. The processed image covers a ground area approximately 120 km in range by 100 km in azimuth, encompassing numerous large-scale geographic features including mountains, valleys, rivers, and lakes.

Figure 6A displays an X-band image of a region near Calleguas, California collected by the Interferometric SAR for Terrain Elevation (IFSARE) system [2]. The IFSARE system is a dual-channel interferometric SAR built by ERIM International Incorporated and the Jet Propulsion Laboratory under the sponsorship of the Defense Advanced Research Projects Agency (DARPA). It simultaneously generates basic stripmap SAR images at two different depression angles and automatically produces terrain elevation maps from these images. The image in Fig. 6A is a composite image assembled from multiple strips. It covers a ground area of approximately 20 × 20 km. The resolution of collected IFSARE imagery is 2.5 m in range by 0.8 m in azimuth. After several averaging operations (required to improve the fidelity of output digital terrain elevation data) and projection of the image into the nominal ground plane, the intrinsic resolution of the image in Figure 6A is approximately 3.5 m in both range and azimuth. Figure 6B illustrates one way to visualize the corresponding terrain elevation. This type of presentation, known as a shaded relief map, uses a conventional linear mapping to represent the gradient of terrain elevation by

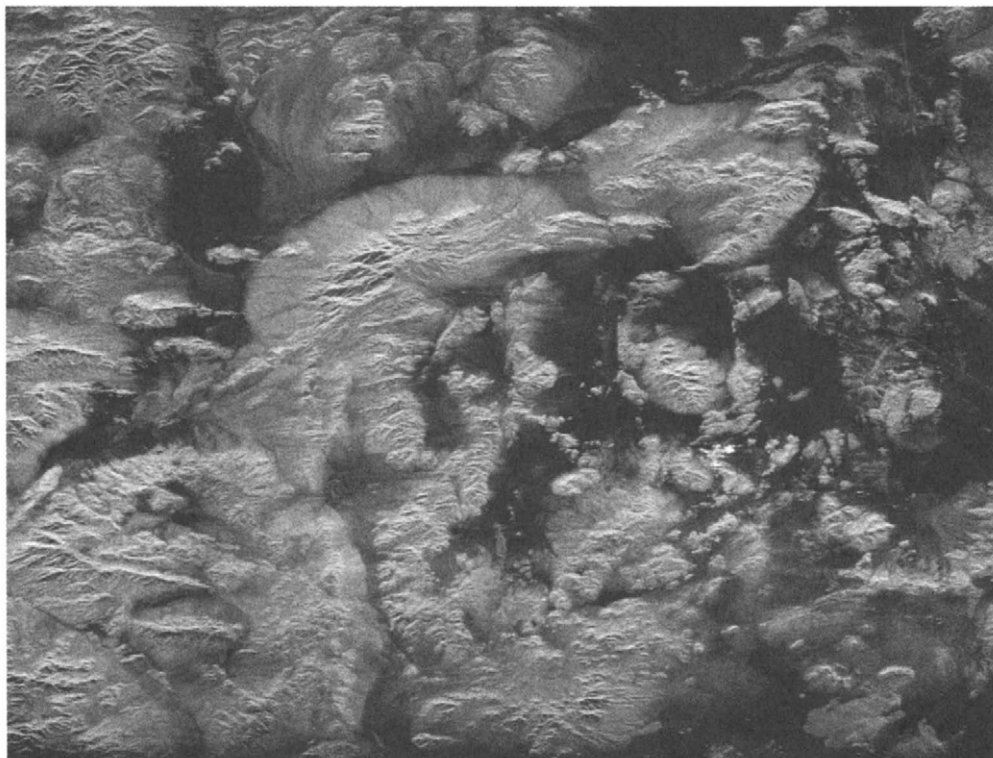


**FIGURE 5** RADARSAT-1 C-band image of Ft. Irwin, California (copyright Canadian Space Agency, 1998).

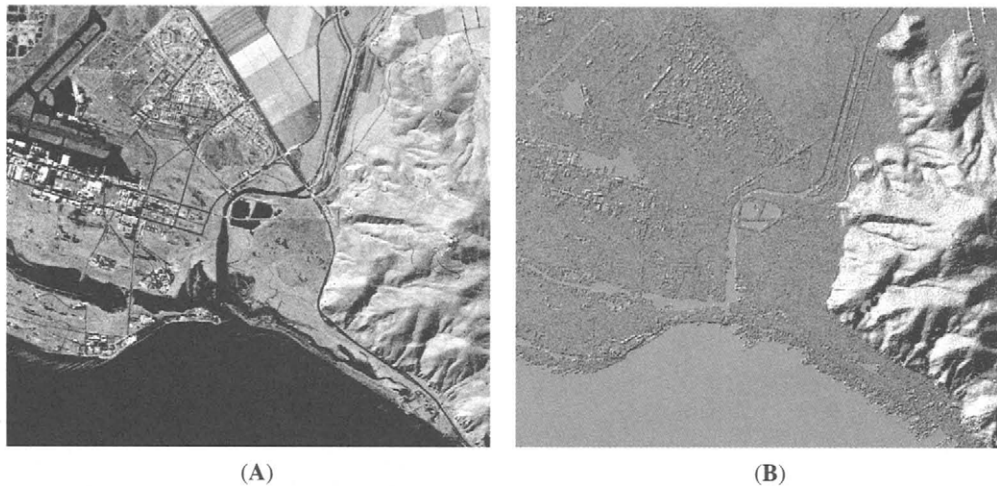


**FIGURE 6** X-band image from the Interferometric synthetic aperture radar (SAR) for Terrain Elevation system: (A) magnitude SAR image of Calleguas, CA; (B) corresponding elevation data displayed as a shaded relief map.

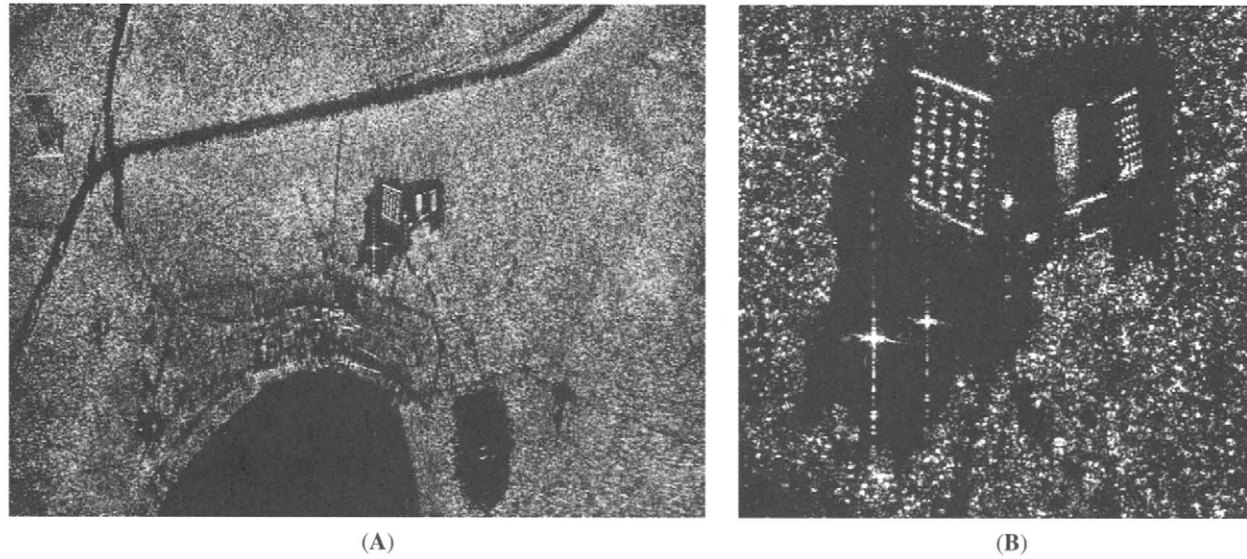


**FIGURE 7** VHF/UHF-band stripmap image of Northern Michigan tree stands: (A) Forested area with several clearings and access roads; (B) close-up view of clearing.

assigning higher gray scale values to steeper terrain slopes. The IFSARE system derives topographic data with a vertical accuracy of 2.0 m or better.

Figure 7A is a fine-resolution VHF/UHF-band image of a forested region in northern Michigan with spatial resolution of 0.33 m in range and 0.66 m in azimuth. This stripmap image originates from an ultrawideband SAR system that flies aboard a U. S. Navy P-3 aircraft. ERIM International designed and built this radar for DARPA in conjunction with the Naval Air Warfare Center (NAWC) for performing foliage penetration (FOPEN) and ground penetration (GPEN) experiments [3]. Figure 7B shows a close-up view of the clearing observed in Fig. 7A. The numerous pointlike scatterers surrounding

the clearing represent the radar signatures of individual tree trunks; a fraction of the incident radar energy has penetrated the forest canopy and returned to the sensor following a double-bounce reflection involving tree trunks and the ground.

The image of the Washington Monument in Fig. 8 originates from the ERIM International airborne Data Collection System [4] operating at X-band in spotlight mode. This 0.3-m-resolution image illustrates the SAR phenomena of *layover* and *shadowing*. Layover occurs because scatterers near the top of the monument are closer to the SAR sensor and return echoes sooner than do scatterers at lower heights. Therefore, the system naturally positions higher scatterers on

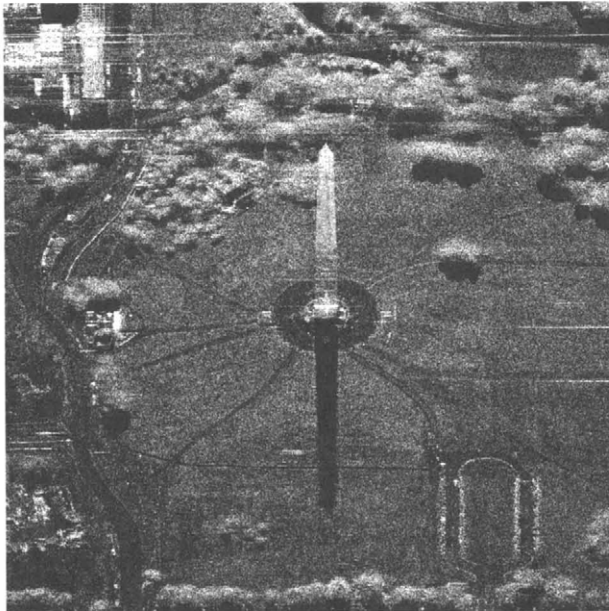


FIGURE 8 Spotlight mode X-band image of Washington Monument collected by the Data Collection System.

a vertical object at nearer ranges (towards the top of Fig. 8) than lower scatterers on the same object. As a result, vertical objects appear to lay over in a SAR image from far range to near range. Shadowing occurs in this example because the monument blocks the illumination of scatterers located behind it. Therefore, these scatterers can reflect no energy back to the sensor. The faint horizontal streaks observed throughout this image represent the radar signatures of automobiles moving with various velocities during the synthetic aperture imaging time. Section 4.1 describes the image characteristics of moving targets.

The spotlight image of the Pentagon in Fig. 9 (from the Data Collection System) illustrates the extremely fine detail that a SAR can detect. Observable characteristics include low return areas, the wide dynamic range associated with SAR imaging, distinct shadows, and individual vehicles in the parking lots. Individual windowsills are responsible for the regular array of reflections observed along each ring of the Pentagon; as in the case of the Washington Monument, they exhibit considerable layover due to their vertical height. It is impressive to realize that SAR systems today can generate such fine-resolution imagery in complete darkness during heavy rain from a distance of many kilometers!

#### 1.4 Characteristics of Synthetic Aperture Radar Signal Data

A SAR sensor transmits a sequence of pulses over time and receives a corresponding set of returns as it traverses its flight path. We visualize this sequence of returns as a 2D signal with one dimension being pulse number (or sensor position



FIGURE 9 Spotlight mode X-band image of Pentagon building collected by the Data Collection System.

along the flight path) and the other being time delay (or round-trip range). Analogous to an optical signal reaching a lens, this 2D radar signal possesses a quadratic phase pattern that the processor must match in order to compress the dispersed signal from each scatterer to a focused point or image of that scatterer. In a simple optical system, a spherical lens provides the required 2D quadratic phase match to focus the incoming field and form an optical image. In a modern SAR imaging system, a digital image formation algorithm generates and applies the required phase pattern. While the incoming SAR signal phase pattern is nominally quadratic in each coordinate, many variations and subtleties are present to challenge the IFP. For instance, the quadratic phase coefficient in the azimuth coordinate varies with the range coordinate or distance to a scatterer. The quadratic phase in the range coordinate is a deterministic function of the linear FM rate of the transmitted radar pulses.

SAR signal data consist of a 2D array of complex numbers. In the range dimension, these numbers result from analog-to-digital (A/D) conversion of the returns from each transmitted pulse. Each sample includes quantized amplitude and phase (or alternatively, in-phase and quadrature) components. In the azimuth dimension, samples correspond to transmitted pulses.

To alleviate high A/D sampling rates, most fine-resolution systems remove the quadratic phase associated with the incoming signals within each received pulse electronically in the receiver before storing the signals. This quadratic phase arises from the linear FM characteristic of the transmitted waveform. Thinking of the quadratic phase in range as a “chirping” signal with a linear variation in frequency over

time, we refer to this electronic removal of the quadratic phase with the terminology *dechirp-on-receive* or *stretch processing*. Following range dechirp-on-receive, the frequency of the resulting intermediate frequency (IF) signal from each scatterer is proportional to the distance from the radar sensor to the scatterer. Figure 10 illustrates this process. Stretch processing is advantageous when the resulting IF signal has lower bandwidth than the RF bandwidth of the transmitted signal.

Similarly, it may be desirable to electronically remove the azimuth quadratic phase (or azimuth chirp) associated with a sequence of pulses in the receiver before storage and subsequent image formation processing. The quadratic phase characteristic in azimuth originates from the quadratic variation in range to each scatterer over the synthetic aperture interval. Processing such a *dechirped* signal in either dimension involves primarily a Fourier transform operation with preliminary phase adjustments to accommodate various secondary effects of the SAR data collection modes and radar system peculiarities. If the radar receiver does not remove these quadratic phase effects, the image formation processor must remove them.

Requirements for a minimum number of range and azimuth samples arise from constraints on the maximum spacing between samples. These constraints are necessary to avoid the presence of energy in the desired image from undersampled signals originating from scatterers outside the scene. The number of complex samples in the range dimension must slightly exceed the number of range resolution cells

represented by the range swath that is illuminated by the antenna elevation beam. Similarly, the number of complex samples in the azimuth dimension must exceed slightly the number of azimuth resolution cells represented by the azimuth extent illuminated by the azimuth antenna beam. In spotlight mode, bandpass filtering in azimuth limits the azimuth scene size and reduces the number of data samples into the IFP.

Signal data include desired signals representing attributes of the scene being imaged, undesired phase effects related to transmitter and receiver properties or to the geometric realities of data collection, phase and amplitude noise from various sources, and ambiguous signals related to inadequate sampling density. Usually, the major error effect in SAR data is phase error in the azimuth dimension arising from uncertainty in the precise location of the radar antenna at the time of transmission and reception of each pulse. Without location accuracy on the order of a fraction of a wavelength, phase errors will exist across the azimuth signal aperture that degrade the quality of the SAR image. Other hardware and software sources of phase errors also are likely even in a well-designed SAR system. Section 3.1 discusses autofocus algorithms to manage these error effects.

## 1.5 Characteristics of Synthetic Aperture Radar Image Data

SAR image data are a 2D array of complex numbers with indices representing, for example, changing range and

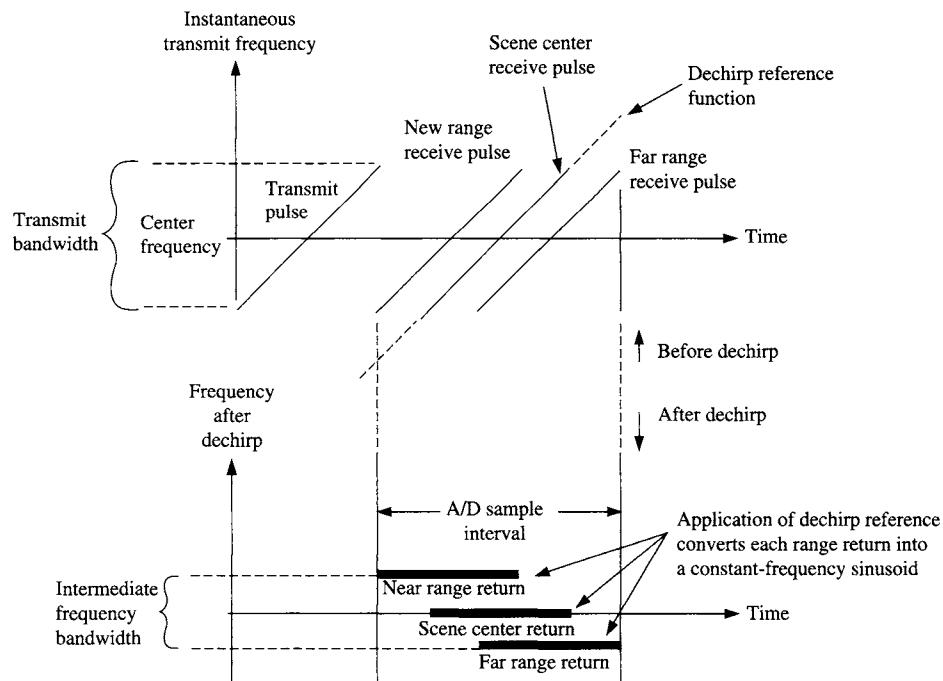


FIGURE 10 Effect of dechirp-on-receive operation on the time/frequency characteristics of radar signals.

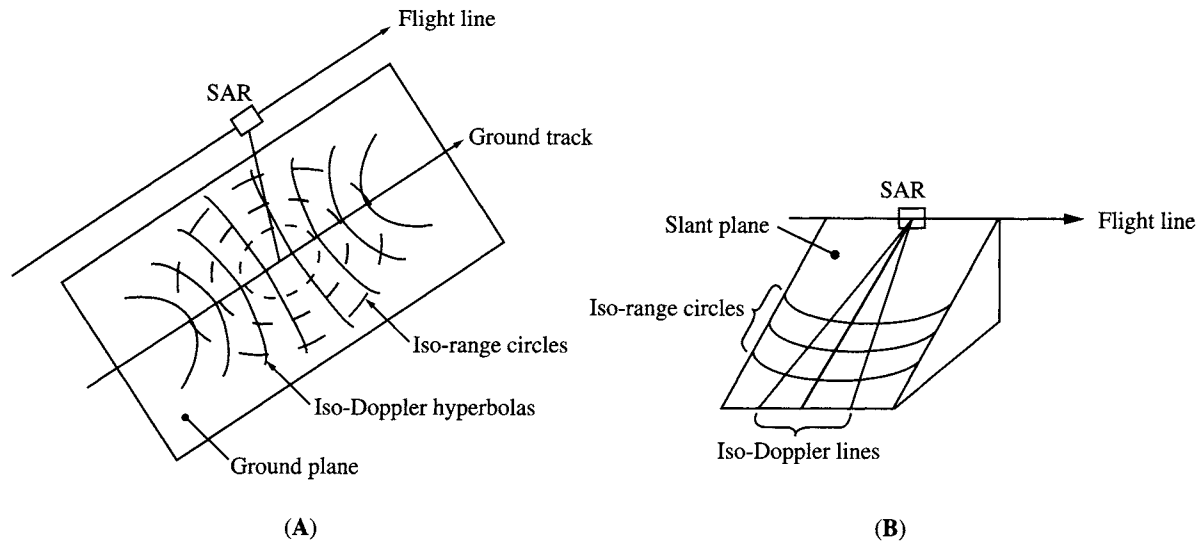


FIGURE 11 Intersection of range spheres with Doppler cones: (A) Ground plane; (B) radar slant plane.

changing azimuth coordinates. Like signal data, each sample includes quantized amplitude and phase (or alternatively, in-phase and quadrature) components. Each element of the array represents an image pixel with amplitude related to the strength of the radar backscatter coefficient in the corresponding scene area. In general, the phase of an image pixel includes a deterministic component and a random component. The deterministic component is related to the distance between the corresponding scatterer and the radar sensor. The random component is related to the presence of many scattering centers over an area the size of a 2D resolution cell in most parts of the scene. Because of this random component, image phase generally is not useful when working with a single image. SAR interferometry, described in Section 4.2, surmounts this difficulty by controlling the data collection environment adequately to achieve (and then cancel) the same random phase component in two images.

Characteristics of radar imagery include center frequency (for instance, X-band or L-band), polarization of transmit and receive antennas (for instance, horizontal or vertical and like or cross polarization), range and azimuth resolutions, and image display plane. Common choices for the image display plane are the nominal ground plane that includes the imaged terrain or the slant plane that contains the antenna velocity vector and the radar line-of-sight vector to scene center. Other attributes of SAR imagery include low return areas (shadows, roads, lakes, and other smooth surfaces), types of scatterers, range layover, targets moving during the data collection, multibounce (multipath) reflections, and coherent speckle patterns. Certain types of scatterers are common to man-made, metallic objects. These types include flat plates, cylinders, spheres, and dihedral and trihedral reflectors. Another type of scatterer is the distributed scatterer containing many scattering centers within the area of a resolution cell, such as a region covered by vegetation or a

large flat roof. Speckle refers to the characteristic nature of radar imagery of distributed scatterers to fluctuate randomly between high and low intensity in radar images. Such fluctuations about an average value appear throughout an otherwise uniform scene because the coherent summation of the echoes from the many scattering centers within each resolution cell yields a random value rather than the mean backscatter coefficient. Speckle is responsible for the mottled appearance of the grassy area surrounding the monument in Fig. 8.

The geometric aspects of SAR image data naturally relate directly to scene geometry, data collection geometry, and sensor parameters. Here we discuss the range and azimuth channels separately to describe these relationships.

Range refers to the distance  $R_t$  between the antenna phase center (APC) and a particular scatterer measured by the time delay ( $t_d = 2R_t/c$ ) between transmission and reception of pulses. Spheres (indicating surfaces of constant range) centered at the APC will intersect a flat earth as circles centered at the radar nadir point. Figure 11A illustrates this geometric relationship. The illuminated parts of each of these circles appear as (straight) lines of constant range in a processed image.

Azimuth relates to angular location in terms of Doppler cone angle, defined as the angle between the antenna velocity vector and the line-of-sight to a particular scatterer. A conical surface (indicating constant azimuth) with its vertex at the APC and its axis along the antenna velocity vector intersects a flat earth as a hyperbola. Figure 11A illustrates the shape of these intersections for a family of conical surfaces. The illuminated parts of each of these intersections appear as (straight) lines of constant azimuth in a processed image.

While a conical surface and a spherical surface centered at the cone vertex intersect orthogonally in 3D space, these circles of constant range and hyperbolas of constant Doppler

on the flat earth generally are not orthogonal. As Fig. 11B illustrates, these intersections are orthogonal in the radar slant plane.

A reasonable set of image quality (IQ) parameters includes resolution, peak sidelobe levels, a measure of additive noise (primarily from thermal noise in the radar receiver), a measure of multiplicative noise, and geometric distortion. Resolution refers to the  $-3\text{-dB}$  width of the mainlobe of the system impulse response. The sidelobe region is the area of the impulse response outside the mainlobe area. Peak sidelobe levels refer to the local peaks in intensity in the sidelobe region. Multiplicative noise refers to signal-dependent effects and includes digital quantization noise, energy in the sidelobes of the system impulse response, and energy from scatterers outside the scene that alias into the image as PRF (pulse repetition frequency) ambiguities. Geometric distortion involves a nonideal relationship between the image geometry and scene geometry, for instance a square patch of terrain taking on a keystone shape in the image.

In practice, requirements on IQ parameters vary among task categories that include terrain imaging, target detection, target classification, and target identification. Each category indicates a different set of image quality, quantity, and timeliness requirements that a SAR system design and implementation must satisfy to perform that task acceptably [5].

## 2 Image Formation Algorithms

This section describes the principal image formation processing algorithms associated with operational spotlight and stripmap modes. We introduce this discussion with a historic review of image formation processing of SAR data.

### 2.1 History of Image Formation Algorithms

The SAR sensor receives and processes analog electromagnetic signals in the form of time-varying voltages. While the modern digital signal processor requires that the receiver sample and quantize these analog signals, the first processor to successfully generate a fully focused SAR image operated on analog signals recorded in a 2D format on a strip of photographic film. In this recording process, the signals returned from successively transmitted pulses were recorded side-by-side parallel to each other along the length of the film in a so-called *rectangular format*. The optical signal processor illuminated the signal film with a coherent (helium neon) laser beam while an assortment of spheric, cylindric, and conical lenses provided the needed quadratic focus to effect a Fourier transform operation. In a perspective analogous to optical imaging, the laser releases the radar wavefronts originating from the illuminated scene and stored in the photographic film while the lenses focus these wavefronts to form a 2D image of the scene. Early digital signal processors performed essentially these same operations on the quantized signals,

mimicking the rectangular format, the quadratic phase adjustments, and the Fourier transform operations inherent in the original optical processor.

Following these early processors, the SAR community has developed a succession of new approaches for processing SAR data to improve image quality, support different data collection modes, and improve algorithm efficiency (particularly with respect to realtime and near-realtime imaging applications). Fortunately, the performance of digital signal processing (DSP) hardware has improved dramatically since the first digital SAR processors to keep pace with increasing processing demands of modern SAR sensors and associated algorithms.

### 2.2 Major Challenges in Synthetic Aperture Radar Image Formation

The generation of high-quality SAR imagery requires that the IFP compensate a number of fundamental effects of radar system design, hardware implementation, and data collection geometry. The more significant effects include scatterer motion through range and azimuth resolution cells, the presence of range curvature, effects of measured sensor motion, errors induced by nonideal sensor hardware components, errors induced by nonideal signal propagation, and errors caused by unmeasured sensor motion. Additional concerns involve computational complexity, quantity of digital data, and data rates.

Of these issues, motion through resolution cells (MTRC) and range curvature usually present the greatest challenges to algorithm design. The remainder of this subsection defines and discusses these two challenges. Together with resolution requirements and scene size, they generally drive the choice of image formation algorithm. In addition, unmeasured sensor motion causes phase errors that often require the use of a procedure to detect, measure, and remove them. Section 3.1 discusses autofocus algorithms to address this need.

Over the synthetic aperture distance necessary to collect the data needed to form a single image, the changing position of the radar sensor causes changes in the instantaneous range and angle from the sensor to any scatterer in the scene being imaged. *Motion through resolution cells* refers to the existence of these changes. Because SAR uses the range and angle to a scatterer to position that scatterer properly within the image, the radar must estimate these changing quantities. For typical narrow-beamwidth sensors, the line-of-sight range to each scatterer is nominally a quadratic function of along-track sensor position. In a generic sense, this variation represents scatterer MTRC in range.

The drawings of imaging geometry in Figure 12 help to relate MTRC to a change in range and define range curvature. In broadside stripmap imaging, the change in range to each scatterer is symmetric about broadside and represents *range curvature*. In a squinted stripmap collection, the variation

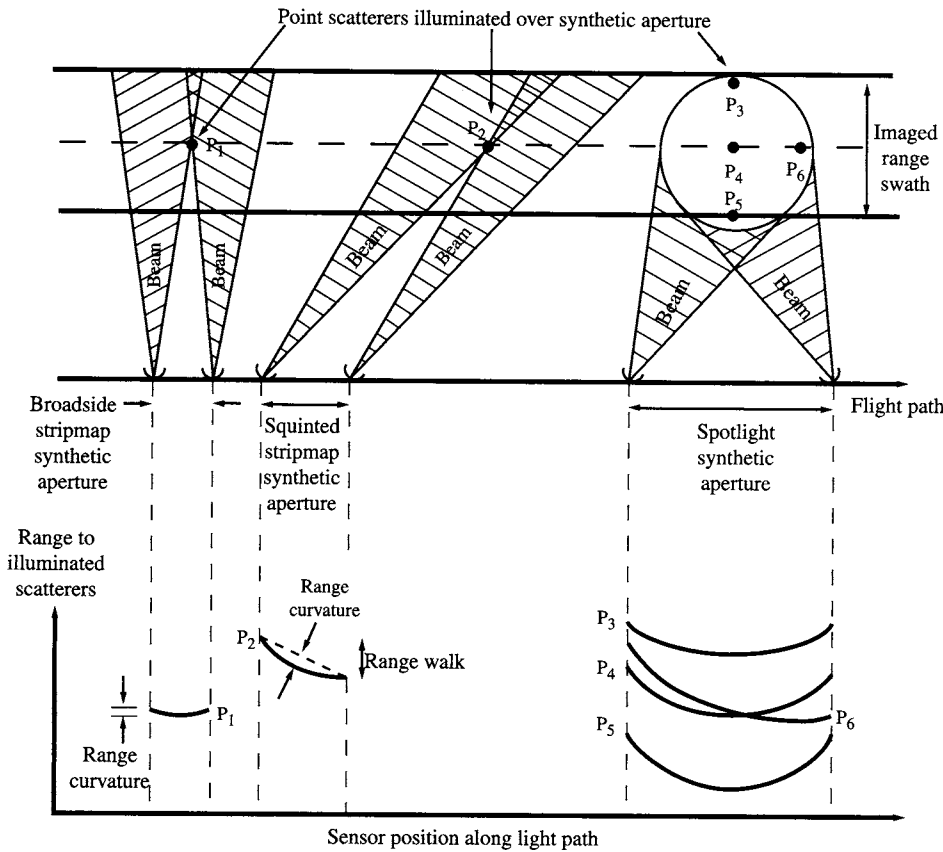


**FIGURE 12** Data-collection geometries showing motion through resolution cells and range curvature including illumination of scatterers (**top**) and the variation in range to scatterers (**bottom**) over stripmap and spotlight synthetic apertures.

in range to each scatterer is not symmetric over the synthetic aperture, but includes a large linear component. The SAR community refers to the linear component as *range walk* and the nonlinear (nominally quadratic) component as *range curvature*. Somewhat different terminology applies to the same effect in the arena of fine-resolution spotlight mode, where all MTRC becomes *range curvature* regardless of whether the motion is linear or nonlinear. Figure 12 illustrates these effects for a stripmap collection (left side) and a spotlight collection (right side).

The key challenge in SAR image formation is the fact that range curvature varies with scatterer location within the imaged scene. The top-right diagram in Fig. 12 suggests this variation. Although it is easy to compensate range curvature for one scatterer, it can be difficult to compensate adequately and efficiently a different range curvature for each scatterer in the image.

For many systems having fine resolution or a wide swath width, this change in range curvature or *differential range curvature* (DRC) across the imaged swath can be large enough to challenge the approximations that most IFP algorithms use in their analytic basis for compensating DRC. The consequences can include spatially variant phase errors that cause image defocus and geometric distortion.

### 2.3 Image Formation in the Stripmap Mode

In *stripmap* mode, successively transmitted pulses interrogate the strip of terrain being imaged at successively increasing along-track positions as the antenna proceeds parallel to the strip. For image formation in stripmap mode, we discuss range-Doppler processing and the range migration algorithm.

Range-Doppler processing is the traditional approach for processing stripmap SAR data. It involves signal storage in a rectangular format analogous to the early optical stripmap processor described in Section 2.1. While many variations of this algorithm exist, the basic approach involves two common steps. First, the IFP compresses the signal data (pulses) in range. It then compresses the (synthetic aperture) data in azimuth to complete the imaging process. If range curvature is significant, the range-compressed track of each scatterer migrates through multiple range bins requiring use of a 2D matched filter for azimuth compression. Otherwise, use of a one-dimensional (1D) matched filter is adequate. A range-Doppler processor usually implements the matched filter via the fast convolution algorithm involving a fast Fourier transform (FFT) followed by a complex multiply and an inverse FFT. The matched filter easily compensates

the range curvature associated with scatterers at some reference range that is specified in the filter design.

A typical approach to accommodate DRC in range-Doppler processing divides the range swath being imaged into narrow subswaths. This division allows the use of the same matched filter for azimuth compression within each subswath tuned to its midrange, but a different matched filter from subswath to subswath. The IFP applies the same 2D matched filter to all range bins within a specific subswath and accepts a gradual degradation in focus away from midrange. A common criterion allows  $\pi/2$  rad of quadratic phase error and limits the maximum subswath width  $\Delta R$  to

$$\Delta R \leq \frac{8\rho_a^2}{\lambda_c} \quad (3)$$

to avoid significant defocus [6]. As an example, an X-band ( $\lambda_c = 0.03$  m) stripmap SAR with 1.0 m azimuth resolution (requiring an azimuth beam width of 0.015 rad) corresponds to a range subswath width  $\Delta R$  of 267 m.

A common version of the range-Doppler algorithm begins with an FFT of the azimuth chirped data to compensate directly for scatterer migration through range bins via a Doppler-dependent, 1D digital interpolation in range. The idea is to straighten the curved trajectories that each scatterer follows in range-Doppler (frequency) space by resampling the range compressed data. Figure 13 summarizes the steps in this process. This method is useful in processing

medium and coarse resolution SAR data, but has difficulty with either fine-resolution data or data collected in a squinted geometry. While an additional processing stage can perform *secondary range compression* to partially overcome this difficulty, the range migration algorithm and the chirp scaling algorithm offer attractive alternatives for many applications.

The range migration algorithm (RMA) is a modern approach to stripmap SAR image formation [7]. As a key attribute, RMA provides a complete solution to the presence of range curvature and avoids any related geometric distortion or defocus. RMA operates on input data after dechirp-on-receive (described in Section 1.4) in the receiver or subsequent range dechirp in the processor. It requires that the receiver preserve (or that the processor reapply) the natural azimuth chirp characteristics of the collected signals when compensating the received data for random sensor motion. We refer to this procedure of preserving the natural phase chirp in azimuth (common in conventional stripmap imaging) as *motion compensation to a line*.

Figure 14 illustrates the key steps in RMA processing. First, RMA transforms the input signal data (already in the range frequency domain following the receiver dechirp-on-receive operation) into the 2D spatial frequency (or *wavenumber*) domain via a 1D along-track FFT. Operation in this 2D wavenumber domain differentiates RMA from range-Doppler algorithms. Next, a matched filter operation removes from all scatterers the along-track quadratic phase variation and range curvature associated with a scatterer located at swath

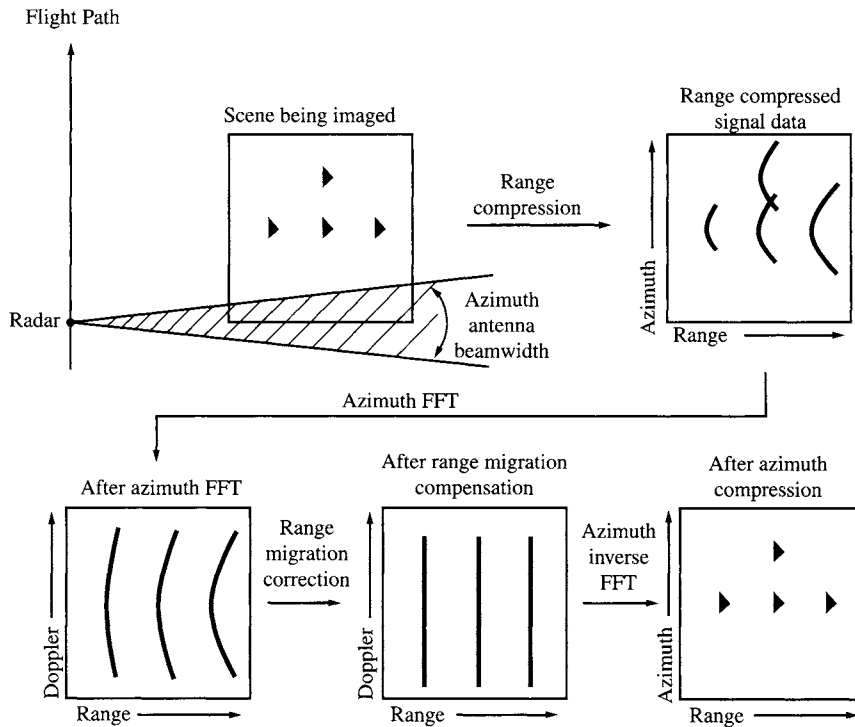


FIGURE 13 Key steps in range-Doppler processing algorithm.

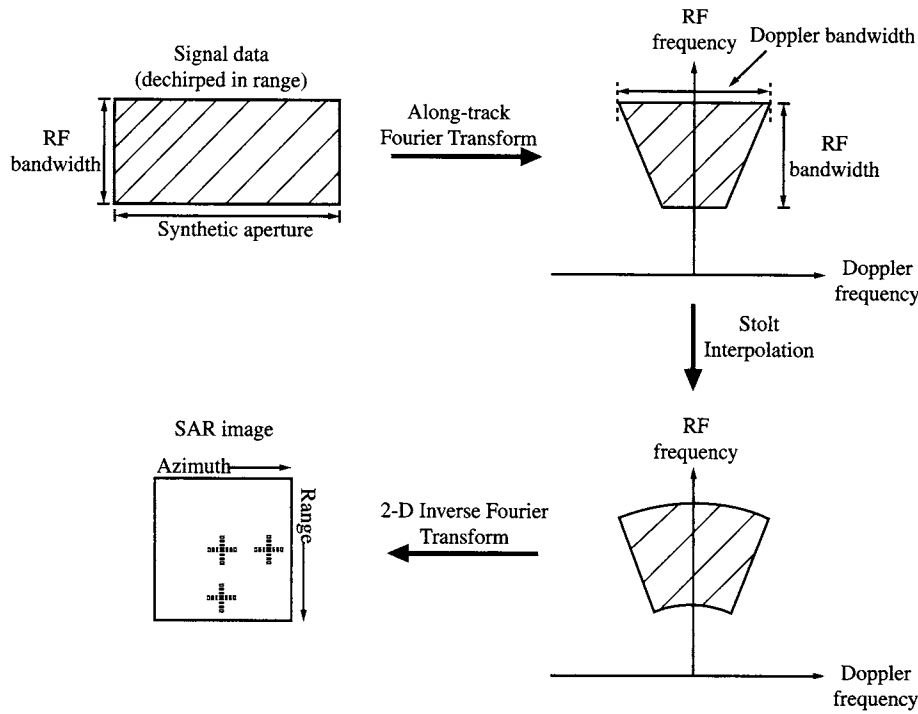


FIGURE 14 Key step in range migration algorithm processing.

center. While this operation perfectly compensates the range curvature of scatterers located along swath center, it provides only partial compensation for scatterers at other ranges. In the next step, a 1D coordinate transformation in the range frequency coordinate (known as the *Stolt interpolation*) removes the residual range curvature of all scatterers. Finally, a 2D inverse FFT compresses the signal data in both range and azimuth to achieve the desired image.

RMA outperforms other algorithms in situations where differential range curvature is excessive. These situations are likely to occur in operations either at fine resolution, with a low center frequency, at a short standoff range, or with a large scene size. Thus, RMA is a natural choice for processing fine-resolution stripmap imagery at VHF and UHF bands for FOPEN applications. With appropriate preprocessing of the signal data, RMA can be a viable choice for spotlight processing applications as well [5].

The chirp-scaling algorithm (CSA) requires SAR input data possessing chirp signal characteristics in both range and azimuth. Related to RMA, CSA requires only FFTs and complex multiplies to form a well-focused image of a large scene; it requires no digital interpolations. This attribute often makes CSA an efficient and practical alternative to RMA.

CSA avoids interpolation by approximating the Stolt transformation step of RMA with a *chirp scaling* operation [5]. This operation applies a Doppler-dependent quadratic phase function to the range chirped data after an FFT of the azimuth chirped data. This process approximately equalizes DRC over the full swath width and permits partial range curvature compensation of all scatterers with a subsequent

matched filtering step. With its efficiency and good focusing performance, CSA and its various extensions have become standard image formation techniques for commercial and scientific orbital SAR systems that operate with coarse to medium resolutions over large swath widths.

## 2.4 Image Formation in the Spotlight Mode

In spotlight mode, successively transmitted pulses interrogate the fixed scene being imaged at successively increasing cone angles as the antenna proceeds past the scene. This vision suggests the storage of collected pulses in a polar format for signal processing. In fact, the polar format algorithm (PFA) is the standard approach for image formation in fine-resolution spotlight mode.

PFA requires SAR signal data after dechirp in range. Such data occur naturally in systems using dechirp-on-receive hardware. Unlike the range migration algorithm, PFA requires that the receiver (or the IFP) remove the natural azimuth chirp characteristics of the collected signals. We refer to this procedure of removing the natural chirp when compensating the received data for random sensor motion as *motion compensation to a point*. This fixed reference point becomes scene center in the spotlight image.

The use of motion compensation to scene center completely removes the effect of MTRC from a scatterer at scene center and partially removes it from other scatterers. PFA removes most of the remaining effects of MTRC by its choice of a data storage format for signal processing. Using a 2D interpolation, the algorithm maps returns from successively transmitted

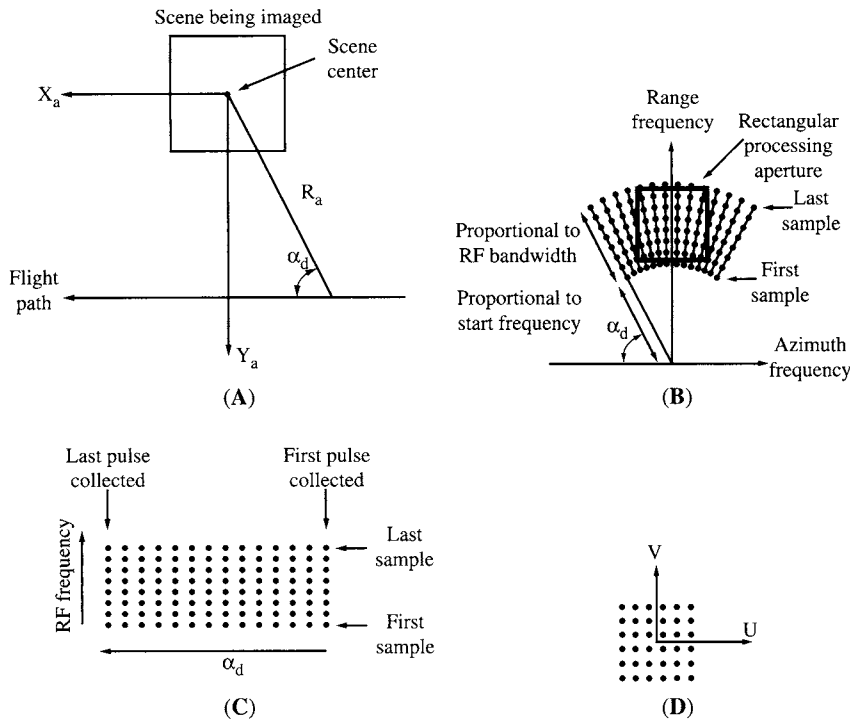


FIGURE 15 Geometric relationships in polar format processing: (A) Slant plane data collection geometry; (B) signal data in rectangular formation; (C) polar formatted signal data; (D) signal data after polar-to-rectangular interpolation.

pulses in an annular shape. It locates each return at a polar angle that tracks the increasing cone angle between the antenna velocity vector and its line-of-sight to scene center as the antenna proceeds past the scene. It locates the returns at a radial distance proportional to the radio frequency of the transmitted pulse. Figure 15 illustrates this data storage format and its similarity to the data collection geometry, particularly in terms of the Doppler cone angle  $\alpha_d$ . The combination of motion compensation to a point and polar formatting leaves a small residual effect of MTRC that we call *range curvature phase error* in discussions of PFA.

Range curvature phase error introduces geometric distortion in the image from residual linear phase effects and causes image defocus from quadratic and higher order phase effects. Based on sensor and data collection parameters, these effects are deterministic and vary in severity over the scene. The digital processor is able to correct the geometric distortion by resampling the processed image to remove the deterministic distortion. The processor cannot easily remove the image defocus resulting from range curvature because the amount of defocus varies over the scene. Because the amount of defocus increases with distance from scene center, the usual method of dealing with it is simply to limit the processed scene to a size that keeps defocus to an acceptable level. A typical criterion allows  $\pi/2$  rad of quadratic phase error. This criterion restricts the allowable scene radius  $r_o$  to

$$r_o \leq 2\rho_a \sqrt{\frac{R_{ac}}{\lambda_c}} \quad (4)$$

where  $R_{ac}$  is the midaperture range between scene center and the SAR antenna [5]. As an example, a system design using  $\lambda_c = 0.03$  m,  $\rho_a = 0.3$  m and  $R_{ac} = 10$  km limits  $r_o$  to 346 m.

To process a larger scene, it is common to divide the scene into sections, process each section separately, and mosaic the sections together to yield an image of the entire illuminated scene. This subpatch processing approach can become inefficient because the IFP must process the collected signal data multiple times in order to produce the final output image. Amplitude and phase discontinuities are invariably present at section boundaries. Significant amplitude discontinuities affect image interpretability, while phase discontinuities impact utility in interferometry and other applications that exploit image phase.

PFA requires a 2D interpolation of digitized signal data to achieve the polar storage format. The IFP typically implements this 2D interpolation separably in range and azimuth via two passes of 1D finite impulse response filters [5].

PFA is an important algorithm in fine-resolution SAR image formation because it removes a large component of MTRC in an efficient manner. In addition, PFA is attractive because it can perform numerous secondary compensations along the way. These compensations include range and azimuth down-sampling to reduce computational load, autofocus to remove unknown quadratic errors, and resampling to change the image display geometry. As a result, use of PFA is common in many operational reconnaissance SAR systems.

### 3 Image Enhancement

The magnitude and phase of each image pixel can have significance in image exploitation. Additionally, the geometric relationship (mapping) between image pixel location and scatterer location in 3D target space is an important aid in target detection, classification, and identification applications. It is the function of image enhancement algorithms to improve or accentuate these image characteristics for image understanding and information extraction.

The complex nature of the SAR image extends the capability of image enhancement algorithms to vary the quality and nature of the image. Important enhancement functions include autofocus, impulse response shaping, geometric distortion correction, intensity remapping, and noncoherent integration. Autofocus and distortion correction improve image quality by addressing deficiencies in the image formation process. Impulse response shaping and intensity remapping provide a capability to adjust image characteristics to match a specific application. Noncoherent integration smoothes speckle noise by noncoherently summing multiple images of the same scene collected at different frequencies or cone angles.

These image enhancement functions are standard considerations in SAR image improvement. In this section, we describe autofocus algorithms and impulse response shaping in detail and briefly discuss the remaining image enhancement functions.

#### 3.1 Autofocus Algorithms

The synthetic aperture achieves fine cross-range resolution by adjusting the relative phase among signals received from various pulses and coherently summing them to achieve a focused image. A major source of uncertainty in the relative phase among these signals is the exact location of the radar antenna at the time of transmission and reception of each pulse. Location accuracy on the order of a fraction of a wavelength is necessary, perhaps to a few millimeters in the case of X-band operation at 10-GHz center frequency. Without this location accuracy, phase errors will exist across the azimuth signal aperture and cause image distortion, defocus, and loss of contrast. Other hardware and software sources of phase error also are likely to be present even in a well-designed system.

The high probability of significant phase error in the azimuth channel of a SAR system operating at fine resolution (typically better than 1-m azimuth resolution) necessitates the use of algorithms during or following image formation to measure and remove this phase error. We refer to the process that automatically estimates and compensates for phase error as *autofocus*. We describe two common autofocus algorithms in this chapter, the mapdrift algorithm and phase gradient autofocus (PGA). The mapdrift algorithm is

ideal for detecting and removing low-frequency phase error that causes image defocus. By low frequency, we mean phase error that varies slowly (for example, a quadratic or cubic variation) over the aperture. PGA is an elegant algorithm designed to detect both low-frequency phase error and high-frequency phase error that varies rapidly over the aperture. High-frequency phase error primarily degrades image contrast.

Originating at Hughes Aircraft Corporation in the mid 1970s, the mapdrift algorithm became the first robust autofocus procedure to see widespread use in operational SAR systems. While mapdrift estimates quadratic and cubic phase errors best, it also extends to higher frequency phase error [9]. With the aid of Fig. 16, we illustrate use of the mapdrift concept to detect and estimate an azimuth quadratic phase error with center-to-edge phase of  $Q$  over an aperture of duration  $T_a$ . This error has the form  $\exp(j2\pi k_q x^2)$  where  $x$  is the azimuth coordinate and  $k_q$  is the quadratic phase coefficient being measured. In its quadratic mode, mapdrift begins by dividing the signal data into two halves (or subapertures) in azimuth, each of length  $T_a/2$ . Mapdrift forms separate, but similar, images (or *maps*) from each subaperture. This process degrades the azimuth resolution of each map by a factor of two relative to the full-aperture image. Viewed separately over each subaperture, the original phase effect includes identical constant and quadratic components but a linear component of opposite slope in each subaperture. Mapdrift exploits the fact that each subaperture possesses a different linear phase component. A measurement of the difference between the linear phase components over the two subapertures leads to an estimate of the original quadratic phase error over the full aperture. The constant phase component over each subaperture is inconsequential, while the quadratic phase component causes some defocus in the subaperture images that is not too troublesome.

By the Fourier shift theorem, a linear phase in the signal domain causes a proportional shift in the image domain. By estimating the shift (or *drift*) between the two similar maps, the mapdrift algorithm estimates the difference in the linear phase component between the two subapertures. This difference is directly proportional to  $Q$ . Most implementations of mapdrift measure the drift between maps by locating the peak of the cross-correlation of the intensity (magnitude squared) maps. After mapdrift estimates the error, a subsequent step removes the error from the full data aperture by multiplying the original signal by a complex exponential of unity magnitude and phase equal to the negative of the estimated error. Typical implementations improve algorithm performance by iterating the process after removing the current error estimate. Use of more than two subapertures to extend the algorithm to higher frequency phase error is rare because of the availability of more capable higher order techniques, such as the PGA algorithm.

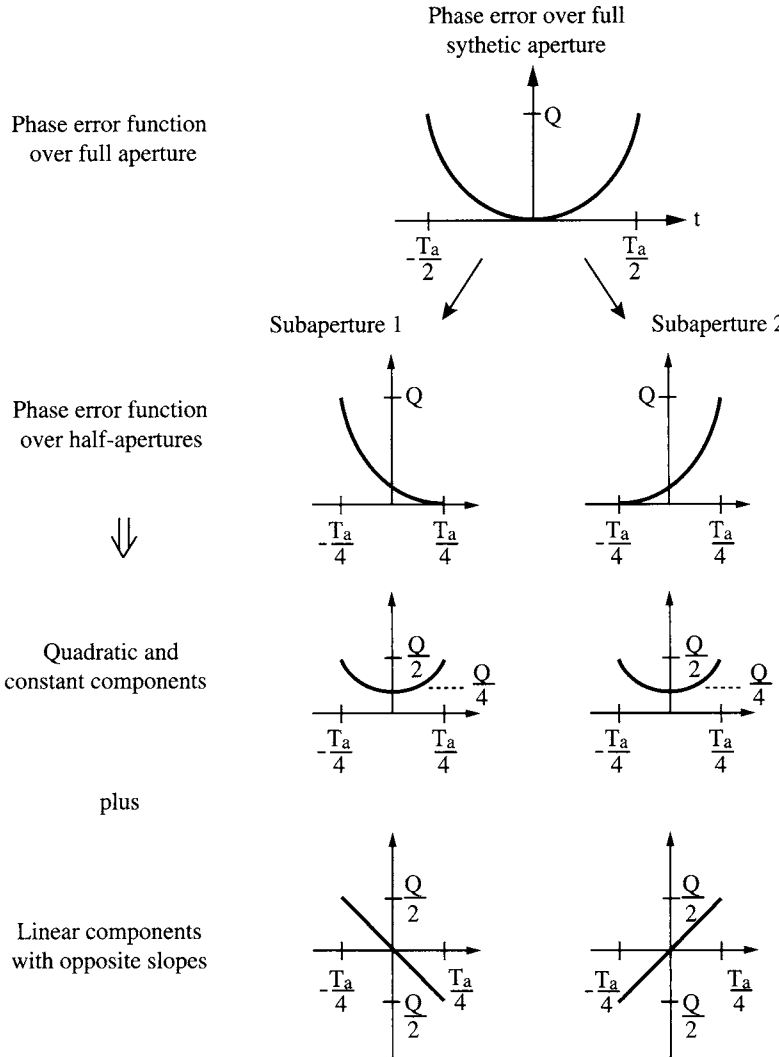


FIGURE 16 Subaperture phase characteristics in mapdrift concept.

The PGA entered the SAR arena in 1989 as a method to estimate higher order phase errors in complex SAR signal data [10, 11]. Unlike mapdrift, PGA is a nonparametric technique in that it does not assume any particular functional model (for example, quadratic) for the phase error. PGA follows an iterative procedure to estimate the derivative (or *phase gradient*) of a phase error in one dimension. The underlying idea is simple. The phase of the signal that results from isolating a dominant scatterer within an image and inverse Fourier transforming it in azimuth is a measure of the azimuth phase error in the signal data.

The PGA iteration cycle begins with a complex image that is focused in range but possibly blurred in azimuth by the phase error being estimated. The basic procedure isolates (by windowing) the image samples containing the azimuth impulse response of the dominant scatterer within each range bin and inverse Fourier transforms the windowed samples. The PGA implementation estimates the phase error in azimuth by measuring the change (or gradient) in phase

between adjacent samples of the inverse transformed signal in each range bin, averaging these measurements over all range bins, and integrating the average. The algorithm then removes the estimated phase error from the original SAR data and proceeds with the next iteration. A number of techniques are available for selecting the initial window width. Typical implementations of PGA decrease the window width following each iteration of the algorithm.

Figure 17 demonstrates use of PGA to focus a 0.3-m resolution stripmap image of the University of Michigan engineering campus. The image in Fig. 17A contains a higher order phase error in azimuth that seriously degrades image quality. Figure 17B shows the focused image that results after three iterations of the PGA algorithm. This comparison illustrates the ability of PGA to estimate higher order phase errors accurately. While the presence of numerous dominant scatterers in this example eases the focusing task considerably, PGA also exhibits robust performance against scenes without dominant scatterers.

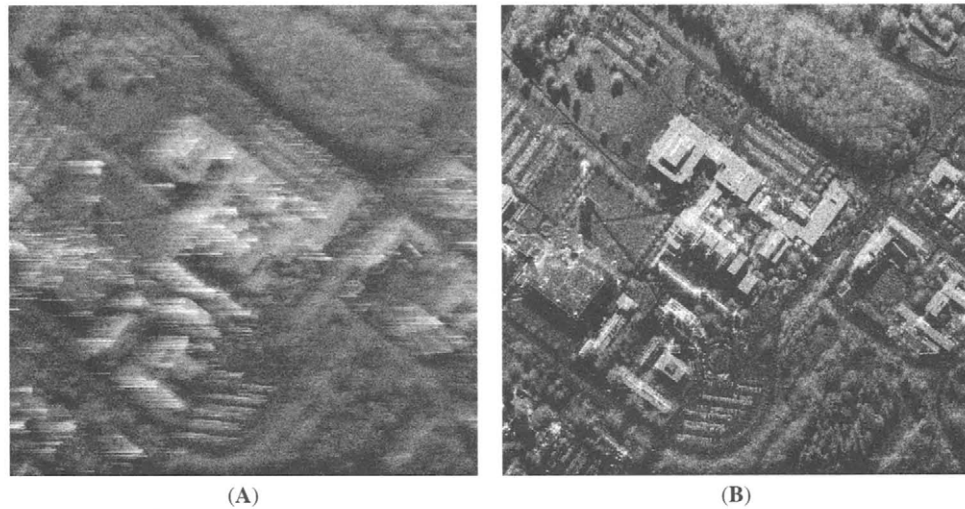


FIGURE 17 Phase gradient autofocus algorithm example: (A) Input image degraded with simulated phase errors; (B) output image after autofocus.

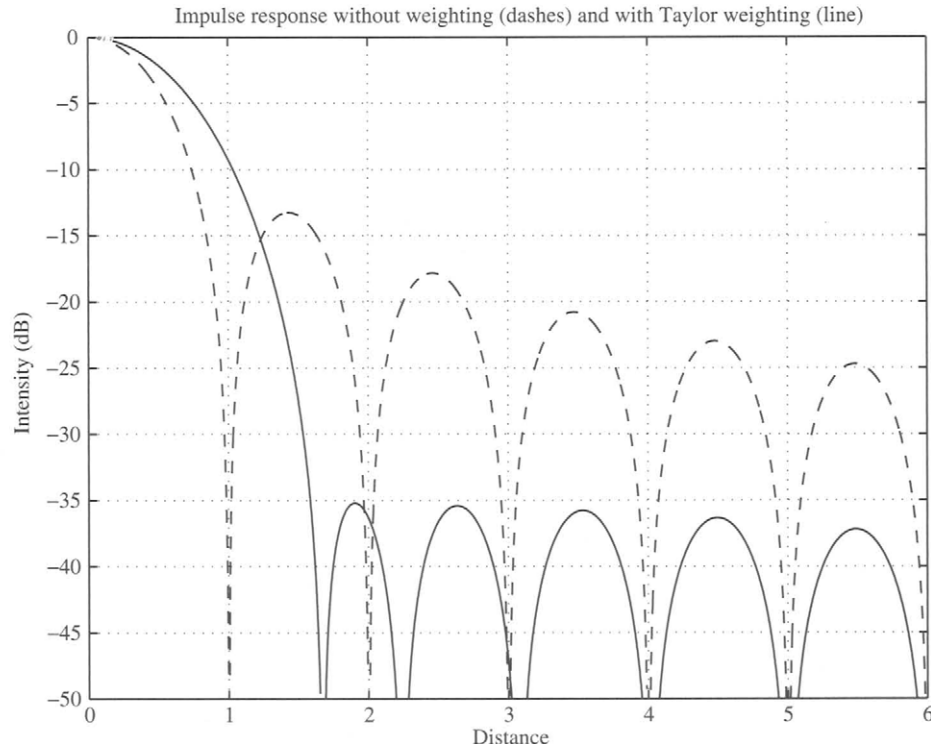
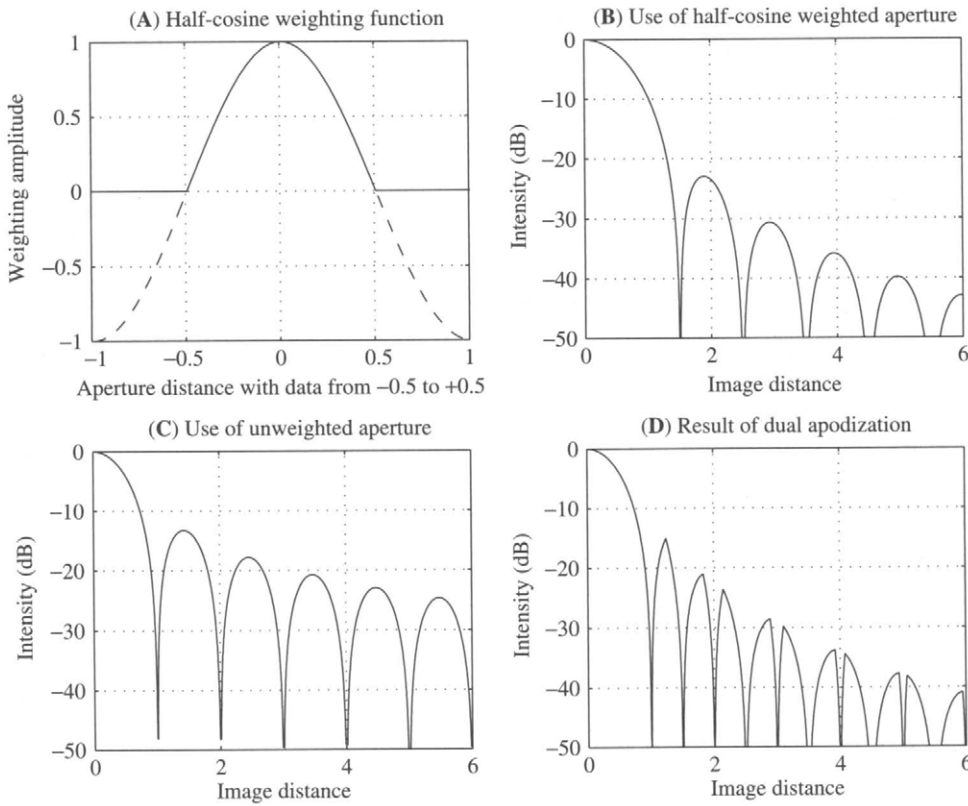


FIGURE 18 Effect of Taylor weighting on mainlobe width and sidelobe levels.

### 3.2 Impulse Response Shaping

In the absence of errors, the impulse response of the SAR imaging system is the Fourier transform of the aperture weighting function. An unweighted (constant amplitude and phase) aperture yields a  $\sin(x)/x$  impulse response. Control of the sidelobes of the impulse response is important to maintain image contrast and avoid interference with weaker

nearby targets by a stronger scatterer. Conventional aperture weighting generally involves amplitude tapering at the data aperture edges to reduce their contribution to sidelobe energy. This type of weighting always widens the mainlobe as a consequence of reducing the energy in the sidelobes. Widening the mainlobe degrades resolution as measured by the  $-3\text{-dB}$  width of the impulse response function. Figure 18 compares the intensity impulse responses from an unweighted



**FIGURE 19** Impulse response comparison using dual apodization (half-cosine).

aperture and from  $-35$ -dB Taylor weighting, a popular choice for fine-resolution SAR imagery. With this weighting function, the first sidelobe is  $35$  dB below the mainlobe peak compared to  $13$  dB without weighting. The weighted  $-3$ -dB main lobe width is  $1.3$  times that in the unweighted case.

Dual apodization is a new approach to impulse response shaping for SAR imagery [12, 13]. In this approach, an algorithm generates two images from the same signal data, one using an unweighted aperture and one using heavy weighting that suppresses sidelobes and widens the mainlobe width. Logic within the algorithm compares the magnitude of the unweighted image with that resulting from the heavy weighting on a pixel-by-pixel basis. This logic saves the minimum value at each pixel location to represent that pixel in the output image. In this way, dual apodization attempts to preserve both the narrow width of the unweighted aperture and the low sidelobe levels of the weighted aperture.

Our example of dual apodization compares the unweighted image with that resulting from half-cosine weighting, which we select specifically for use in a dual apodization operation. Figure 19A illustrates the half-cosine weighting. Alone, half-cosine weighting is not useful because it greatly degrades the mainlobe of the impulse response. However, as a partner in dual apodization with the unweighted aperture, it performs adeptly to minimize sidelobes without increasing mainlobe width. Figures 19B and 19C show the unweighted and

weighted impulse responses. Unlike many aperture-weighting functions that do not significantly change the zero-crossings of the impulse response function, half-cosine weighting does shift the zero-crossings relative to those of the unweighted aperture. Figure 19D indicates the impulse response resulting from dual apodization. This result maintains the width of the unweighted aperture and the sidelobe levels of the half-cosine weighted aperture. Dual apodization with this pair of weightings requires that we multiply the magnitude of the weighted image by a factor of two before comparison to balance the reduction in amplitude from weighting. Figure 20 compares a SAR image containing a number of strong targets using an unweighted aperture and using this dual apodization pairing.

Space variant apodization (SVA) is a step beyond dual apodization that uses logic queries regarding the phase and amplitude relationships among neighboring pixels to determine whether a particular pixel consists of primarily mainlobe energy, primarily sidelobe energy or a combination of the two [12, 13]. The logic directs the image enhancement algorithm to zero out the sidelobe pixels, maintain the mainlobe pixels, and suppress the pixels of mixed origin. The operation of SVA to zero out sidelobe pixels introduces some suppression of clutter patterns. Reference [12] supplements the original papers with heuristic explanations of SVA and SAR image examples.

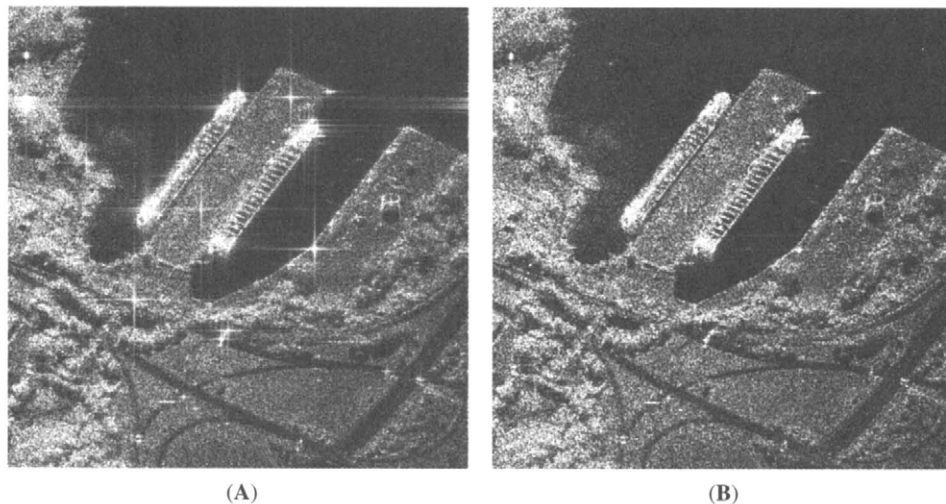


**FIGURE 20** Image example using dual apodization: (A) Original image with unweighted aperture; (B) image with dual apodization (half-cosine).

### 3.3 Other Image Enhancement Functions

Other image improvement options include geometric distortion correction, intensity remapping, and noncoherent integration. Geometric distortion refers to the improper positioning of scatterers in the output image with respect to their true position when viewed in a properly scaled common image display plane. Correction procedures remove the deterministic component of geometric distortion by resampling the digital SAR image from distorted pixel locations to undistorted locations. Intensity remapping refers to a (typically) nonlinear transformation between input pixel intensity values and output intensity. Such a remapping operation is particularly important when displaying SAR imagery in order to preserve the wide dynamic range inherent in the digital image data (typically 50 to 100 dB). Noncoherent integration refers to a process that detects the amplitude of SAR images (thereby eliminating the phase) and averages a number of these detected images taken at slightly different cone angles in order to reduce the variance of the characteristic speckle that naturally occurs in SAR images.

Geometric distortion arises largely from an inadequacy of the IFP algorithm to compensate for the geometric relationships inherent in the range/angle imaging process. When necessary to satisfy image quality requirements, an image enhancement module after image formation compensates for deterministic distortion by interpolating between sample points of the original image to obtain samples on an undistorted output grid. This digital resampling operation (or interpolation) effectively unwarps the distorted image in order to reinstate geometric fidelity into the output image.

Intensity remapping is necessary and valuable because the wide dynamic range (defined as the ratio between system noise and the highest intensity scatterer present) inherent in radar imagery greatly exceeds that of common display

media. It is often desirable to examine stronger targets in their natural background of terrain or in the presence of weaker targets. The common approach to remapping sets input pixels below a lower threshold level to zero, sets input pixels above an upper threshold level to that level, and maps pixels in between from input to output according to a prescribed (generally nonlinear) mapping rule. One popular remapping rule performs a linear mapping of image pixels having lower intensity and a logarithmic mapping of pixels having higher intensity. The output of this *linlog* mapping is typically an image with 8-bit samples that retains the proper linear relationship among the intensities of low-level scattering sources (such as terrain), yet compresses the wide dynamic range of the strongest scatterers (typically man-made, metallic objects).

Noncoherent integration (or multilook averaging) of fine-resolution radar images allows the generation of radar images with an almost optical-like appearance. This process smoothes out the pixel-to-pixel amplitude fluctuations (speckle noise) associated with a coherent imaging system. By including scatterers sensed at a multitude of cone angles, it adds detail to the target signature to enhance identification and provide a more literal image appearance. Figure 21 shows a fine-resolution SAR image of an automobile resulting from noncoherent summation of 36 images collected at unique cone angles.

## 4 Image Exploitation

The value of imagery is in its use. Information inherent in image data must be identified, accessed, quantified, often calibrated, and developed into a usable and observable form. Observation may involve visual or numeric human study or automatic computer analysis.

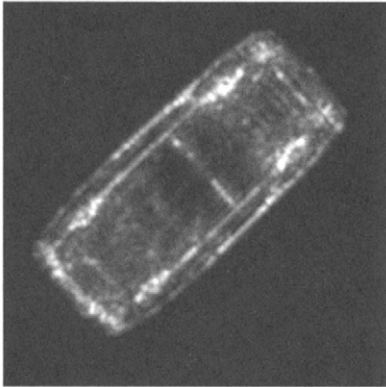


FIGURE 21 Use of noncoherent integration to reduce speckle noise and fill in target signature.

An image naturally presents a spatial perspective to an observer with a magnitude presentation of specific features or characteristics. Beyond this presentation, SAR image data offers additional information related to its coherent nature, with meaningful amplitude and phase associated with each pixel. This complex nature of SAR imagery represents special value when the image analyst can relate it to target or data collection characteristics of value in specialized military or civilian applications.

Some examples of these special applications of SAR image data include moving target detection (possibly with tracking and focusing) using a single image and digital terrain elevation data (DTED) extraction via interferometry using multiple images collected at different depression angles. We discuss these two applications in detail below.

Additional applications of a single SAR image include glint detection, automated road finding and following, and shadow exploitation. Glints (or specular flashes) refer to bright returns off the edges of linear surfaces, characteristic of man-made structures such as aircraft wings. Road finding and shadow detection naturally involve searches for low return areas in the image. Additional applications involving multiple images include target characterization using polarization diversity and change detection using images of the same area collected at different times from a similar perspective. Differences in signatures from both terrain and cultural features as a function of the polarization characteristics of transmit and receive antennas support target classification and identification tasks. Change detection generally involves the subtraction of two detected images collected at different times. Image areas that are unchanged between collections will experience significant cancellation while features that have changed will not cancel, making the changes easier to identify.

## 4.1 Moving Target Detection

Target motion during the coherent aperture time used to generate azimuth resolution disturbs the pulse-to-pulse phase

coherence required to produce an ideal impulse response function. The result is azimuth phase error in the signals received from moving target scatterers. In conventional SAR imagery, such phase error causes azimuth smearing of the moving target image. In the simple case of a target moving at constant velocity parallel to the antenna path (along-track velocity) or at constant acceleration toward the antenna (line-of-sight acceleration), the phase error is quadratic and the image smearing is proportional to the magnitude of the motion [5]. This image effect offers both a basis for detection of a moving target and a hope of refocusing the moving target image after image formation [14]. In the simple-motion case presented here, the image streak corresponding to a moving scatterer possesses a quadratic phase in the image deterministically related to the value of the target motion parameter and to the quadratic phase across the azimuth signal data. This quadratic phase characteristic of the streaks in the image offers an interesting approach to automatic detection and refocusing of moving targets in conventionally processed SAR images.

Equations relating target velocity to quadratic phase error in both domains and to streak length are well known [5]. A target moving with an along-track velocity  $V_{tat}$  parallel to the antenna velocity vector introduces a quadratic phase error across the azimuth signal data. The zero-to-peak size  $Q_{Vtat}$  of this phase effect is

$$Q_{Vtat} = \frac{\pi V_{tat} T_a}{2 \rho_a S_{\alpha c}} \quad (5)$$

Here,  $T_a$  is the azimuth aperture time and  $S_{\alpha c}$  is the sine of the cone angle at aperture center.

Conventional image formation processing of the resulting signal data produces an azimuth streak in the image for each scattering center of the target. The length  $L_s$  of each streak is roughly

$$L_s = \frac{2 V_{tat} T_a}{S_{\alpha c}} \quad (6)$$

Each image streak has a quadratic phase characteristic along its length of the same size but opposite sign as the phase effect in the signal data before the Fourier transform operation that produces the image. Figure 22 indicates these relationships. Line-of-sight target acceleration introduces a similar quadratic phase effect, while more complicated motions introduce higher order (for example, cubic, quartic and sinusoidal) phase effects.

A simple algorithm for automated detection of moving target streaks in conventional SAR imagery utilizes this low-frequency (largely quadratic) phase characteristic of the image streaks representing moving target scatterers. The procedure is to calculate the pixel-to-pixel change in phase in the

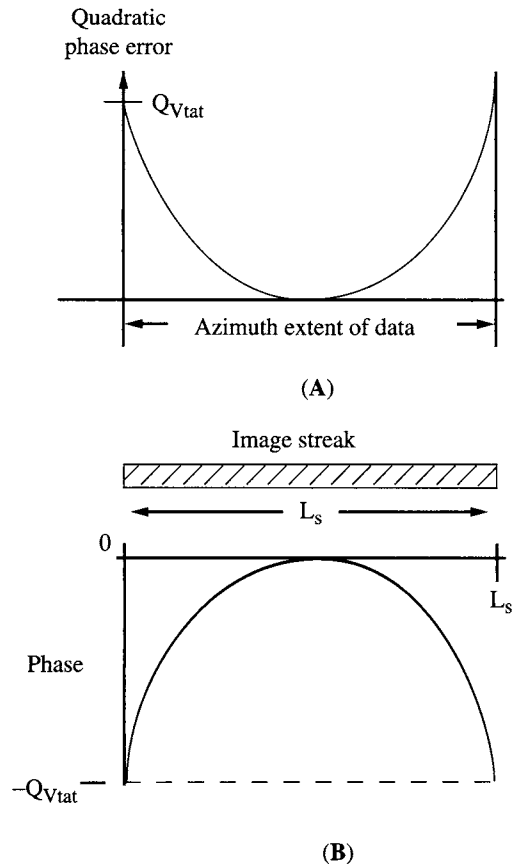


**FIGURE 22** Characteristics of moving target signals: (A) Phase associated with signal data; (B) phase along image data.

azimuth direction along each range bin of the image. Normal stationary SAR image background areas including stronger extended targets such as trees and shrubbery vary almost randomly in phase from pixel to pixel while the streaks associated with moving scatterers vary more slowly and regularly in phase. This smooth phase derivative from azimuth pixel to azimuth pixel differentiates moving scatterers from stationary scatterers in a way easily detected by an automated process.

Figure 23A displays a 0.3-m resolution SAR image that includes a group of streaks associated with a defocused moving target. In this image, the horizontal coordinate is range and the vertical coordinate is azimuth. The moving target streaks are the brighter returns extending over much of the azimuth extent of the scene. The phase along each streak is largely quadratic. Figure 23B displays the azimuth derivative of the phase of this image from  $-\pi$  change (dark) to  $+\pi$  change (light). Various averaging, filtering, and thresholding operations in this phase derivative space will easily and automatically detect the moving target streak in the background. For instance, one simple approach detects areas where the second derivative of phase in azimuth is small.

A measure of  $L_s$  in Fig. 23, along with Equations 10.1.5 and 10.1.6, provides an estimate of the quadratic defocus parameter associated with this image. A moving target focus algorithm can make this estimate of defocus and apply a corrective phase adjustment to the original signal data to improve the focus of this moving target image. Ideally, this process generates a signature of the moving target identical

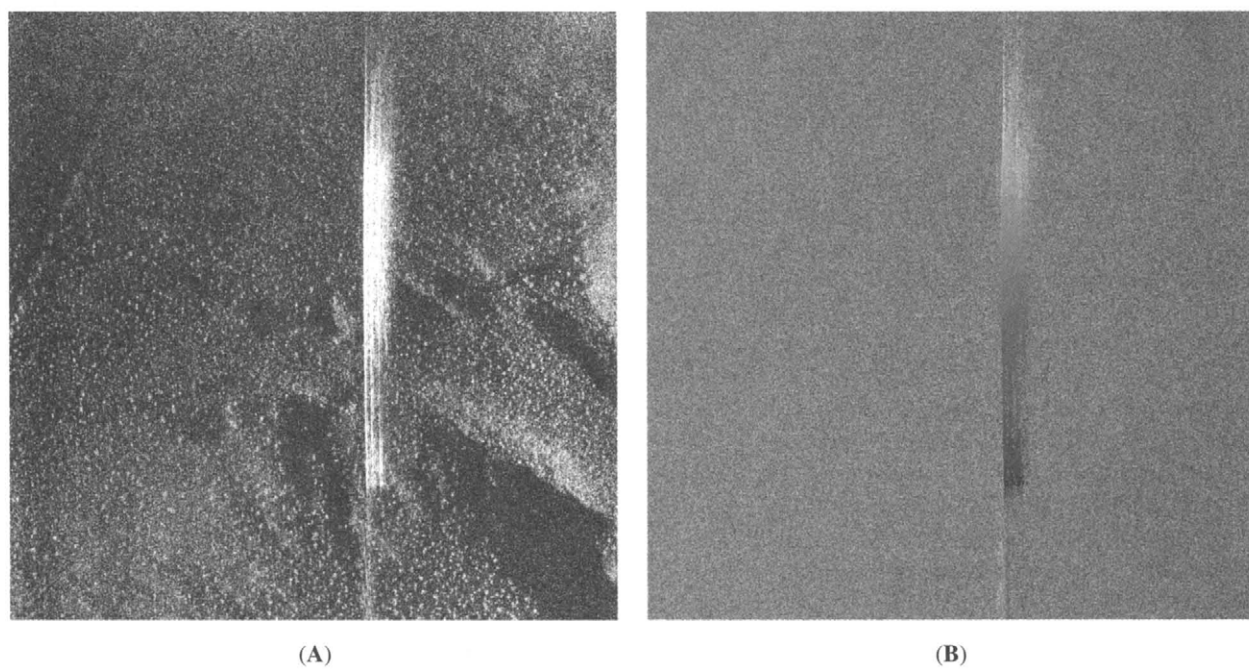


**FIGURE 23** Example of moving target detection: (A) Synthetic aperture radar image with moving target present; (B) phase derivative of image.

to that of a similar stationary target. In reality, target motion is significantly more complex than that modeled here. In addition, the moving target streaks often do not stand out as well from the background as they do in this particular image. However, sophisticated implementations of this simple algorithm can provide reasonable detection performance even for a relatively low ratio of target streak intensity to background intensity.

## 4.2 Synthetic Aperture Radar Interferometry

SAR interferometry requires a comparison of two complex SAR images collected over the same Doppler cone angle interval but at different depression angles. This comparison provides an estimate of the depression angle from the sensor to each pixel in the image. Figure 24A illustrates an appropriate data collection geometry using a vertical interferometer

(second antenna directly below first antenna). Information on the depression angle from the sensor to each pixel in the image, along with the cone angle and range provided by a single SAR image, locates scatterers in three dimensions relative to the sensor location and velocity vector. With information about these sensor parameters, absolute height and horizontal position is available to generate a digital terrain elevation map. A natural product of SAR interferometry is a height contour map. Figure 6 presents example products from a modern interferometric SAR system. Major applications encompass both civilian and military activities.

We use the vertical interferometer in Fig. 24A to illustrate the geometric basis for determining depression angle. The image from the first antenna locates the scatterer P<sub>1</sub> on the range-Doppler circle C<sub>1</sub> in a plane orthogonal to the sensor velocity vector. The image from the second antenna locates P<sub>1</sub> on the range-Doppler circle C<sub>2</sub>. The point P<sub>2</sub> is the center

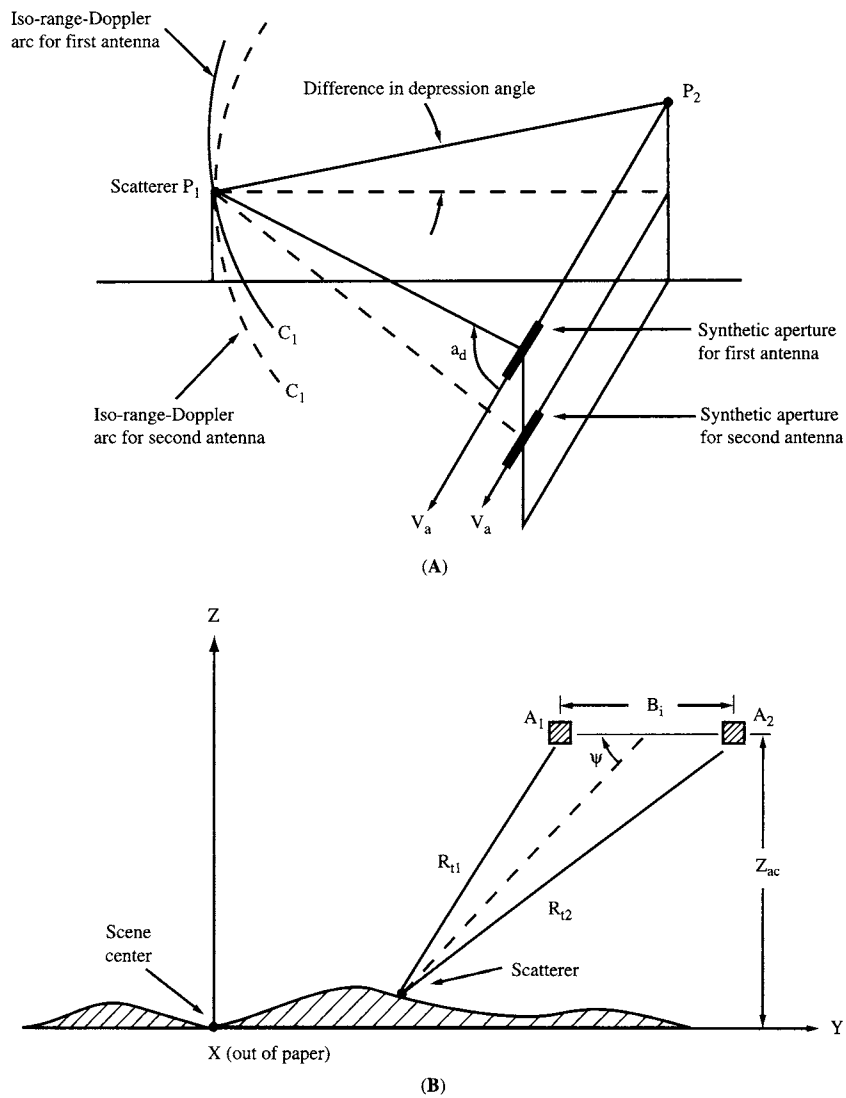


**FIGURE 24** Geometric models for synthetic aperture radar (A) Basis for estimating depression angle; (B) model for interferometric analysis.

of both circles. In the absence of errors, the intersection of the two circles identifies the location of P1.

The mathematic basis and sensitivity of SAR interferometry is readily available in the published literature [15–17]. To summarize the equations that characterize the interferometric SAR function, we use the horizontal interferometer illustrated in Fig. 24B. The two antennas A1 and A2 are at the same height. They are separated by a rigid baseline of length  $B_i$  orthogonal to the flight line. Each antenna illuminates the same ground swath in a broadside imaging direction. The sensor travels in the X direction,  $\psi$  is the nominal depression angle from the interferometer to the scatterer relative to the horizontal baseline and  $Z_{ac}$  is the height of the interferometer above the nominal ground plane XY.

Following image registration, multiplication of the first image by the complex conjugate of the second image yields the phase difference between corresponding pixels in the two images. For a particular scatterer, this phase difference is proportional to the difference in range to the scatterer from each antenna. This range difference,  $R_{t1} - R_{t2}$  in Fig. 24B, is adequate information to determine the depression angle to the scatterer. Without resolving the natural  $2\pi$  ambiguity in the measurement of phase, this phase difference provides an estimate of only the difference in depression angle between the scatterers represented by image pixels rather than their absolute depression angle. The relationship between relative depression angle  $\Delta\psi$  and the difference  $\Delta\phi_{12}$  between pixels in this phase difference between images is

$$\Delta\psi = \frac{-\lambda_c \Delta\phi_{12}}{4\pi B_i \sin(\psi)} \quad (7)$$

Two pixels with an interferometric phase difference  $\Delta\phi$  differ in depression angle by  $\Delta\psi$ . A change in  $\Delta\phi_{12}$  corresponds to a change in height  $\Delta h$  given by [5].

$$\Delta h = -K_h \Delta\phi_{12} \quad (8)$$

with

$$K_h = -\frac{\lambda_c Z_{ac} \cot(\psi)}{4\pi B_i \sin(\psi)} \quad (9)$$

As an example, we consider an interferometer with horizontal baseline  $B_i = 1$  m, center frequency  $\lambda_c = 0.03$  m, operating at a depression angle  $\psi = 30$  degrees from a height  $Z_{ac} = 4$  km. We have the coefficient  $K_h = -33.1$  m/rad =  $-0.58$  m/degree; thus 10 degrees of interferometric phase difference corresponds to 5.8 m of height change.

## 5 Chapter Summary

Microwave imaging has been an attractive technology since its early roots in the World War II era largely because of

its potential for 24-hour remote surveillance in all weather conditions. In recent years, particularly with the advent of the synthetic aperture radar approach to realizing fine azimuth resolution, microwave imagery has come to represent a powerful remote sensing capability. With today's fine-resolution SAR techniques, the finest radar imagery begins to take on the appearance of optical imagery to which we are naturally accustomed. For many applications, the utility of SAR imagery greatly exceeds that of comparable optical imagery.

Four factors contribute significantly to this advanced state of radar imaging. First, advances in SAR sensor hardware technology (particularly with respect to resolving capability) provide the inherent information within the raw SAR data received by the radar sensor. Second, recent developments in image formation algorithms and computing systems provide the capability to generate a digitized image in a computationally efficient manner that preserves the inherent information content of the raw radar signals. A combination of requirements on airborne SAR for finer and finer resolution in various military applications and requirements on orbital SAR for wide-area coverage in natural resource and environmental applications provided the impetus for these developments. Third, improvements in image quality via state-of-the-art image enhancement algorithms extend the accessibility of information and emphasize that information of interest to the specialized user of SAR imagery. Autofocus and space-variant apodization exemplify these image quality improvements. Finally, an explosion in powerful exploitation techniques to extract information coded in the phase as well as the amplitude of SAR imagery multiplies the value of the radar imagery to the end user.

## Acknowledgment

---

The image in Figure 5 is copyright Canadian Space Agency, 1998. All other SAR images are courtesy of General Dynamics Advanced Information Systems.

## References

- [1] R. K. Raney, A. P. Luscombe, E. J. Langham, and S. Ahmed, "RADARSAT," *Proc. IEEE* 79 (1991).
- [2] G. T. Sos, H. W. Klimach, and G. F. Adams, "High performance interferometric SAR description and capabilities," *Proc. 10<sup>th</sup> Thematic Conference on Geologic Remote Sensing* San Antonio, TX May 9–12 (1994).
- [3] D. R. Sheen, S. J. Shackman, N. L. Vanden Berg, D. L. Wiseman, L. P. Elenbogen, and R. F. Ranson, "The P-3 ultra-wideband SAR: description and examples," *Proc. 1996 IEEE National Radar Conference* Ann Arbor, MI (1996).
- [4] M. A. DiMango, W. T. Hanna, and L. Andersen, "The data collection system (DCS) airborne platform," *Record of the First International Airborne Remote Sensing Conference and Exhibition* Strasbourg, France, (1994).

- [5] W. G. Carrara, R. S. Goodman, and R. M. Majewski, *Spotlight Synthetic Aperture Radar: Signal Processing Algorithms* (Artech House, Boston, MA, 1995).
- [6] J. C. Curlander and R. N. McDonough, *Synthetic Aperture Radar: Systems and Processing* (Wiley, New York, 1991).
- [7] F. Rocca, C. Cafforio, and C. Prati, "Synthetic aperture radar: a new application for wave equation techniques," *Geophys. Prospect.* 37, 809–830 (1989).
- [8] R. K. Raney, H. Runge, R. Bamler, I. G. Cumming, and F. H. Wong, "Precision SAR processing using chirp scaling," *IEEE Trans. Geosc. Remote Sens.* 32, 786–799 (1994).
- [9] C. E. Mancill and J. M. Swiger, "A map drift autofocus technique for correcting higher order SAR phase errors (U)," *27<sup>th</sup> Annual Tri-Service Radar Symposium Record* Monterey, CA, June 23–25 (1981).
- [10] P. Eichel, D. Ghiglia, and C. Jakowatz, Jr., "Speckle processing method for synthetic aperture radar phase correction," *Opt. Lett.* 14 (1989).
- [11] D. E. Wahl, P. H. Eichel, D. C. Ghiglia, et al., "Phase gradient autofocus—a robust tool for high resolution SAR phase correction," *IEEE Trans. Aerospace Electr. Syst.* 30, 827–834 (1994).
- [12] H. C. Stankwitz, R. J. Dallaire, and J. R. Fienup, "Spatially variant apodization for sidelobe control in SAR imagery," *Proc. 1994 IEEE National Radar Conference* (1994).
- [13] H. C. Stankwitz, R. J. Dallaire, and J. R. Fienup, "Nonlinear apodization for sidelobe control in SAR Imagery," *IEEE Trans. Aerospace Electr. Syst. AES-31*, 267–279 (1995).
- [14] S. Werness, W. Carrara, L. Joyce, et al., "Moving target imaging algorithm for SAR data," *IEEE Trans. Aerospace Electr. Syst., AES-26*, 57–67 (1990).
- [15] E. Rodriguez and J. M. Martin, "Theory and design of interferometric synthetic aperture radars," *IEEE Proc.* 139, 147–159 (1992).
- [16] H. Zebker and R. M. Goldstein, "Topographic mapping from interferometric synthetic aperture radar observations," *J. Geophys. Res.* 91, 4993–4999 (1986).
- [17] H. Zebker and J. Villasenor, "Decorrelation in interferometric radar echoes," *IEEE Trans. Geosc. Remote Sens.* 30, 950–959 (1992).